

## Non-intrusive characterization of the hall thruster azimuthal drift current

Cliff A. Thomas, Nicolas Gascon, and Mark A. Cappelli  
Mechanical Engineering Department  
Stanford University, Stanford CA 94305-3032

A plasma diagnostic is developed for the non-invasive study of the azimuthal drift in an axially symmetric  $E \times B$  discharge plasma - that of a Hall thruster. Typical Hall plasmas are characterized by strongly magnetized electrons and streaming ions, and it is hoped that a better understanding of the azimuthal drift in such devices might reveal the importance of various mechanisms on bulk electron mobility in the broader range of  $E \times B$  discharge plasmas. In this study the technique of fast current interruption is used to generate near-field signals across a set of loop antenna encircling the outer insulating  $Al_2O_3$  channel walls of a Hall thruster. The derivative signal is interrogated to determine the magnitude and distribution of azimuthal drift within the channel walls. The results of the non-intrusive antenna experiment are compared with an estimate derived via intrusive methodologies, and it is found that the intrusive measurements lead to an underestimate of the Hall dipole. Lastly, the steady-state magnetic field perturbation (from the vacuum measured value) attributable to the azimuthal drift is approximated with the method of finite elements at 160V and 200V discharge. In comparison to the vacuum magnetic field it is found that the region of maximum radial magnetic field in the operating Hall thruster shifts towards the anode and experiences a reduction in magnitude in upwards of 12% for the operating conditions tested.

### I. INTRODUCTION

The use of a loop antenna external to the outer dielectric wall for the non-invasive investigation of the azimuthal drift current in an  $E \times B$  discharge is a diagnostic whose initial development dates to the mid 1970's and perhaps even earlier [1, 2]. In these prior studies it was implemented to estimate the total azimuthal drift current and its "center of gravity" in a coaxial Hall discharge. These measurements have been validated to a significant degree by complementary antenna measurements [3], 1-D and 2-D numerical codes, and a host of more invasive probing techniques [4]. The use of the loop antenna to investigate the drift current in an  $E \times B$  discharge is predicated upon several simple notions: (i) that the loop antenna is an excellent indicator for local oscillating magnetic dipoles of antenna-comparable spatial scales; (ii) that the bandwidth of the loop antenna's response is wide (and easily predicted for a wide variety of boundary conditions); (iii) that the antenna is easily fabricated with considerable gain, and (iv) that the geometry of the coaxial discharge is easily lent to a axially symmetric treatment favorably matched by practical constraints on loop antenna design, implementation, and analysis.

A loop antenna array is a natural extension of this diagnostic given that the response of any particular antenna is dependent on the orientation and precise location of any neighboring

transmitting magnetic dipoles. Under the constraints that the receiving and transmitting components are collinear, the problem of determining the spatial location and magnitude of a distribution of oscillating dipoles is considerably simplified. Given that the azimuthal perturbations in the Hall thruster's drift current are expected to be negligible with respect to the total drift at any given axial position, the drift current is considered to generate a finite dimension magnetic dipole that can be investigated with an antenna array.

The antenna array is combined with the technique of fast current interruption, which involves commutating the anode potential on a timescale shorter than that characterizing plasma relaxation. In turning off the discharge the  $E \times B$  drift is zeroed, and an electromagnetic transient is generated which propagates to the antenna array. The proper placement of the antenna array and the use of the time  $\rightarrow \infty$  boundary condition (that the azimuthal drift decays to zero) allow a determination of the state of the azimuthal drift at the moment of current interruption.

### II. EXPERIMENTAL SETUP

#### II.1. Stanford Hall Thruster (SHT)

The  $E \times B$  plasma discharge used in this study is a laboratory version of a low-power Hall thruster (<1 kW), details regarding which can be found in existing publications [5-7]. The source consists of an annular  $Al_2O_3$  channel 90mm in

diameter, 11mm in width, and 80mm in length. The magnetic circuit consists of four outer coils, one inner coil, and three iron plates providing a radial magnetic field whose peak in vacuum is 5mm upstream of the exit plane. Details regarding the magnetic circuit are also available in previously published literature [7]. A hollow stainless steel ring with 32 equidistant holes (0.5mm in diameter) serves as the anode and propellant feed. A commercially available hollow cathode (Ion Tech HCN-252) provides electrons for neutralizing the ion beam.

## II.2. Vacuum Chamber

The experiments reported here were performed in a 3.25m long stainless steel vacuum chamber 1.25m in diameter with a pressure of  $10^{-5}$ mbar (as measured using an uncorrected ion gauge) during nominal operation of the thruster. This was accomplished using two CVI cryogenic pumps (model number TM1200) with liquid nitrogen shrouds. Separate DC power supplies were used for the discharge, cathode keeper, cathode heater, and electromagnetic coils. The cathode was kept at tank potential (ground). Measurements of the discharge current were made using a powered differential amplifier (Tektronix P5200) placed across a  $4\Omega$  load in series with the discharge. Measurements of the antenna response were captured using two digital oscilloscopes that could be simultaneously triggered from a signal proportional to the discharge current (a Tektronix TDS 3014 and a Tektronix TDS 3054). As a result, the response from six separate antennas could be co-located in time.

## II.3. Fast Switch

In order to accomplish fast current interruption a manually controlled power MOSFET was placed in series with the discharge. It was controlled using floating CMOS logic components. In this manner current commutation in 200-400ns was achieved.

## II.4. Antenna Array

To precisely align and maintain the position of several antennae with respect to the discharge channel, six tracks were cut in a Teflon sleeve sized to just clear the outer diameter of the ceramic wall. The spacing of the tracks was 1.6 mm, and they were sized to tightly secure 0.5 mm diameter Kapton insulated magnet wire. With the wire antennae in place (and each connected to a matching  $50\Omega$  cable with BNC termination) the entire assembly was thinly coated with a commercially available BN spray

to help resist the chamber environment. One end of the antenna array was polished so that it could be positioned next to the magnetic pole piece at the exit plane (by abutting it) with as little error as possible. Surface interference was measured to be  $\sim 0.2$  mm, and this was included in all relevant computations. A picture of the final antenna assembly and a diagram of the antenna placement are shown in Figs. 1 and 2.

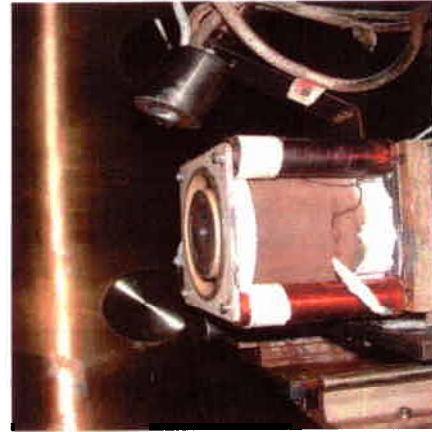


Figure 1. The antenna assembly appears as a white ring abutting the magnetic pole piece on the SHT.

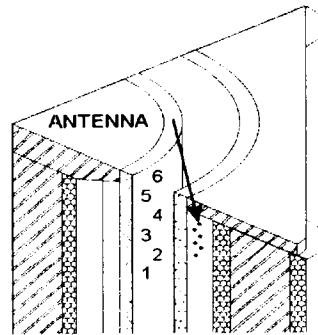


Figure 2. The location of the antenna array with respect to a quarter section of the SHT.

## III. AZIMUTHAL DRIFT DIAGNOSTIC

### III.1. Problem Formulation

Determining the azimuthal drift from the antenna array's temporal response requires an inverse solution to Maxwell's field equations. To solve for the voltage induced in a pickup coil Maxwell's equations must be satisfied consistent with the boundary conditions. The problem is aided by axial symmetry and several approximations.

Faraday's Law of induction can be written utilizing the axial symmetry of the discharge and Stokes' Theorem (provided that transients are of a timescale that a voltage,  $V$ , can be properly defined for the relevant length scale) to provide an integral formula more readily related to the experimentally measured antenna response, i.e.,

$$V = -\frac{\partial}{\partial t} \oint (H + M) \cdot \hat{n} dA \quad (1).$$

Here,  $H$  is the magnetic field strength, and  $M$  is the magnetization of the medium, which must be determined by the full solution of Maxwell's equations. In its most basic form, Eqn. 1 can be represented by a Green's function solution in frequency space, with the contribution  $\delta V_\omega$  to the total voltage  $V$  in the coil located at  $\vec{x}$  arising from a current density  $J_\theta$  at position  $\vec{x}'$  as

$$\delta V_\omega(\vec{x}) = -G_\omega(\vec{x}, \vec{x}') \left[ \frac{\partial J_\theta(\vec{x}', t)}{\partial t} \right]_\omega \delta A(\vec{x}') \quad (2).$$

In this expression,  $\delta A(\vec{x}')$  is a differential area element normal to the azimuthal direction at the axial position  $\vec{x}'$ , and  $G_\omega$  is the associated Green's function. Eqn. 2 is the preferred launching point for the inverse problem, as the unknown current density can be approximated to a specifiable set of functional parameters. The forward and reverse problem herein considered depends on the strict applicability of frequency superposition as implied in Eqn. 2 – an equation for which non-linearity can arise due to the variable magnetic permeability of iron (a primary component in the magnetic circuit). It is assumed (and later verified) that the Hall current causes only minor perturbations in the magnetization of the poles. An error due to mode interaction is therefore assumed to be negligible.

### III.2. Special Considerations

It is important to note that the experimentally measured voltage will also depend on the self-inductance of the pickup coil. If  $\phi$  is the voltage induced across a small but finite air gap in the antenna's length due to a change in area-integrated flux, the measured voltage must be corrected by

$$\phi_\omega = (i\omega L_\omega + Z_\omega) I_\omega \quad (3).$$

In Eqn. 3,  $Z_\omega$  is the oscilloscope impedance (usually  $50\Omega$ ),  $I_\omega$  is the loop current, and  $L_\omega$  is the impedance of the loop antenna. For most frequencies the self-inductance is small, and at high frequencies the effective self-inductance is reduced below expected levels due to shielding by neighboring conducting surfaces. For the purposes of this study it was found that the antennas' self-inductances were negligible (as verified by experimental measurement and numerical calculation), and at frequencies of 50MHz a correction of only 2% was necessary.

The computation of the Green's function is laborious, but must be done precisely to ensure accuracy in the inverse solution to Eqn. 2. In the previous literature the Green's function solution is approximated by experiment [1-3]. A metal loop is placed inside the boundary of interest and a current in the loop is sinusoidally excited in time, or it is excited and/or interrupted on a timescale characteristic of the phenomena that the antenna is intended to study. In this way a rough approximation of  $G_\omega$  for a given spatial position can be found. This procedure is also used here. However, unlike previous studies, a detailed finite element model is also used to numerically determine the frequency dependent Green's function for a multitude of antenna/calibration coil spatial permutations. This was done for two reasons: (i) to more accurately capture differences in  $G_\omega$  due to small changes in spatial location, and (ii), to more accurately capture the physics of the line source and its boundary equations. It is recognized that the *metal* calibration coil itself changes the boundary conditions and at high frequencies its current is rather narrowly confined to its surface (a condition rather different than the homogenous distribution generally assumed for calibration purposes).

The numerical approach to the Green's function calculation is not presented here to save space. In general, the level of agreement between the experimental and numerical calibration techniques was within a few percent - a number well within the error of the laboratory calibration tests.

It is further noteworthy that the presence of the discharge plasma in the actual experiment is assumed to have a negligible impact on the calculations – i.e., quasi-neutral Xe plasma is the working medium, and for frequencies of interest has no appreciable magnetic qualities. Furthermore, though the Xe plasma frequency is much greater than the range of electromagnetic frequencies investigated, the plasma is

sufficiently collisional as to make the effective skin depth far greater than the plasma dimensions. Thus, the Xe is assumed to behave as free space in all numerical computations of the Green's function in Eqn. 2.

### III.3. Fast Current Interruption

To determine the azimuthal drift current and its distribution within the channel the discharge current is commutated on a timescale significantly shorter than the expected plasma relaxation time. The commutation circuit is designed to eliminate the axial electric field (and the azimuthal drift) on a timescale of 200-400 ns. This is significantly shorter than the fastest avenue for electron energy or population loss, including collisional - radiative processes, wall collision/ neutralization, and ionization processes. For example, the electron loss rate due to recombination at the wall can be approximated by considering the time it would take an electron to cross the channel radially, but this is limited by space-charge effects coupled to the ion mass, and so, is not as fast a process as might be anticipated. Assuming that ions entering the sheath are traveling at the Bohm velocity, the relaxation time can be approximated as

$$\tau = \frac{\Delta R}{1.2\sqrt{kT_e/M_i}} \quad (4).$$

Here,  $\Delta R$  is the channel width,  $T_e$  is the electron temperature, and  $M_i$  is the ion mass. For  $\Delta R = 12\text{mm}$  and for a mean electron energy of 10eV,  $\tau$  is estimated to be 3700 ns. Of course, the expected relaxation time is shorter than this due to the combined influence of *all* relevant relaxation processes, but not considerably so. Line-of-sight emission measurements on Hall discharges under similar conditions indicate relaxation times of order 1000ns [3]. As a result, it is assumed that the plasma density is frozen while the azimuthal drift is brought to zero *coherently* across the channel with the anode potential. The antenna response can then be used to study the state of the azimuthal drift at the moment of discharge disruption, and the fact that the azimuthal drift *must* decay to zero serves as a useful temporal boundary condition. By performing repeated tests the average azimuthal drift can be calculated, and an envelope enclosing its *maximum large-scale perturbations* can be found.

The spatial distribution of the drift is found by taking multiple antennas (in this case six) at different locations, and by calculating the infinite time frequency content of their temporal response during a fast current interruption event. A single parameterized function of space and time is fit to Eqn. 2 with the least possible error. In all following computations a five-parameter fit to the spatial distribution for the current density is assumed consisting of a double-Gaussian of unknown center and half-width in two separate dimensions (radial and axial). This approach is chosen because it is consistent with the expected drift profile and, upon analysis, provided the best fit of the functional spaces investigated.

Since fast current interruption effectively enforces the coherent decay of the azimuthal drift across the channel, a simple decomposition of the current density is possible, i.e.,

$$J_\theta = I_\theta X(\vec{x}') T(t) \quad (5).$$

Here,  $T$  is most generally a function of time and space ranging from zero to one, but in this instance is restricted to time.  $X$  is the aforementioned double Gaussian, but normalized such that the integration of  $J_\theta$  across the channel for  $T = 1$  yields the total azimuthal drift current. Substitution of Eqn. 5 into Eqn. 2 yields

$$\delta V_\omega(\vec{x}) = -I_\theta G_\omega(\vec{x}, \vec{x}') X(\vec{x}') \left[ \frac{\partial T}{\partial t} \right]_\omega \delta A(x') \quad (6).$$

Since  $I_\theta \left[ \frac{\partial T}{\partial t} \right]_\omega$  is independent of coil location it is calculated as a function of frequency with an appropriate guess at  $X$

$$I_\theta \left[ \frac{\partial T}{\partial t} \right]_\omega = \frac{\sum_{\vec{x}} -V_\omega(\vec{x})}{\sum_{\vec{x}} \int_{\vec{x}'} G_\omega(\vec{x}, \vec{x}') X(\vec{x}') \delta A(x')} \quad (7).$$

Iteration on  $X$  is accomplished given the result of the above by considering frequencies with mathematically substantial signal integrity (those frequencies whose response significantly exceeds the overlying noise). The parameters of  $X$  are adjusted slightly to reduce the norm of the residual

$$\rho_{\omega}^i = V_{\omega}^i + I \left[ \frac{\partial T}{\partial t} \right]_{\omega} \int_{\bar{x}} G_{\omega}^i(\bar{x}') X(\bar{x}') dA(x') \quad (8).$$

Eqn. 8 applies for the  $i^{\text{th}}$  antenna at a given frequency within the band of relevant frequency response. Note that the components for any given residual are not normalized; as weight should be assigned to those components of any given residual that are inherently larger. Thus, component weighting is proportional to variable magnitude. This process is repeated until convergence is achieved using a steepest descents algorithm.

### III.4. Dynamic Current Oscillation

For the setup considered herein a direct space/time analysis of low frequency perturbations (such as the breathing mode) was impractical, as the antenna array and measurement system did not provide enough gain to produce signals substantially above the system noise at low frequencies. Regardless, the magnitude and distribution of perturbations to the average azimuthal drift can be understood by considering the range of solutions garnered via fast current interruption, since any single solution can be considered to be a snapshot in time of the normal operational envelope.

### III.5. Intrusive Estimate of Azimuthal Drift

Previous experiments at Stanford University [5] coupled with knowledge that the electrons are strongly magnetized allowed an approximation of the azimuthal drift in a simple form

$$J_{\theta} \cong n_e \frac{E_z}{B_r} \quad (9).$$

Here the electron number density is found using a Langmuir probe, the electric field with an emissive probe, and the magnetic field density with a Hall probe (in vacuum).

### III.6. FE Magnetic Field Calculation

In all instances where the magnetic field magnitude is plotted in section IV, the displayed product is courtesy of the freeware 2-D finite element program FEMM [10]. The results of FEMM have been found to match experimentally measured vacuum field values for the SHT to better than 1% (for coarse grids), and quantitatively capture with high detail all

relevant features of the SHT's magnetic field topology.

## IV. EXPERIMENTAL RESULTS

### IV.1. Fast Current Interruption

Four tests were carried out with the anode potential at 160V and four more at 200V. A typical plot of the transient antenna response to a commutation event is shown in Fig. 3.

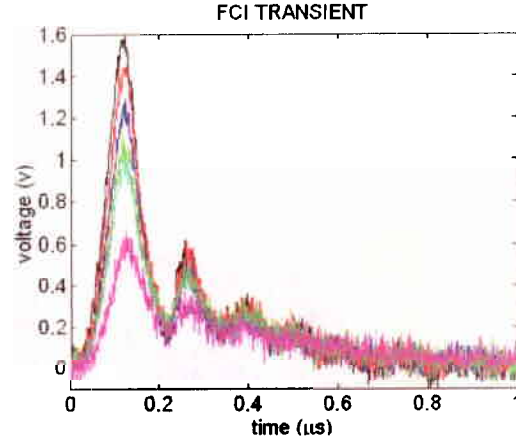


Figure 3. The commutation transient for antennas 1-6 for a 200V discharge.

### IV.2. Distribution of Azimuthal Drift

At 160V the calculated Hall dipole for each of the four tests varied little from the average of 16.6A. The standard deviation in the drift over the four tests was 3.5A, and the time-averaged discharge current for each test was 1.48A. The azimuthal drift and magnetic field magnitude are shown in Fig. 4 and Fig. 5.

The maximum drift is located very near the maximum magnetic field in vacuum – as expected from classical diffusion theory. The maximum magnetic field is located near the exit plane since this is where the poles of the magnetic circuit are located, and is greater on the inner radius due to the gradient in B common to axially symmetric Hall thruster designs (since  $\nabla \cdot B = 0$ ). It is apparent in Fig. 5 that the contribution to the magnetic field of the distributed drift decreases the magnetic field density and shifts the peak magnetic field towards the anode on the channel centerline. This effect will be detailed more precisely in the next section, and supports findings that the magnetic field is perturbed from its vacuum

value during normal operation [8], though not to the extent observed in [8].

At 200V the average Hall dipole was calculated to be 31.8A with a standard deviation in the 4 tests of 9.3A. It is uncertain whether the greater spread at 200V is due to the small sample size, or due to enhanced fluctuations at increased discharge voltage. Previous tests suggest the latter [9]. The time-averaged discharge current for each test was 1.9A. The azimuthal drift and magnetic field magnitude are shown below in Fig. 6 and Fig. 7 for 200V discharge.

At 200V the drift current is significantly larger than at 160V, though its half-width in the radial and axial directions is roughly unchanged as well as its general location. It should be noted that the location accuracy of the drift “center” is roughly 1mm in the radial and/or axial directions for both tests, and this more than obscures the small discrepancy in the findings for figures 4-7 of a slight offset of the relative drift centers. The accuracy of the drift current calculation is limited by the accuracy of the antenna registration, and the level of refinement used in calculating the Green’s functions representing discrete line

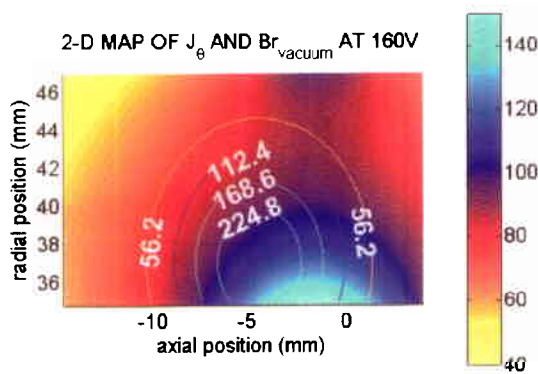


**Figure 4.** The average azimuthal drift and  $|B|$  for 160V discharge. The azimuthal drift is given by the contours in  $(\text{kA}/\text{m}^2)$ . The shaded 2-D background is  $|B|$  in (G).

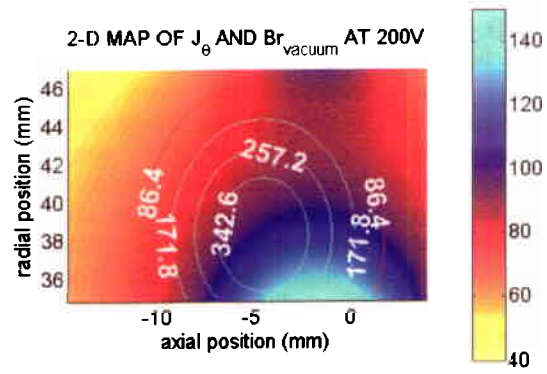


**Figure 6.** The average azimuthal drift and  $|B|$  for 200V discharge. The azimuthal drift is given by the contours in  $(\text{kA}/\text{m}^2)$ . The shaded 2-D background is  $|B|$  in (G).

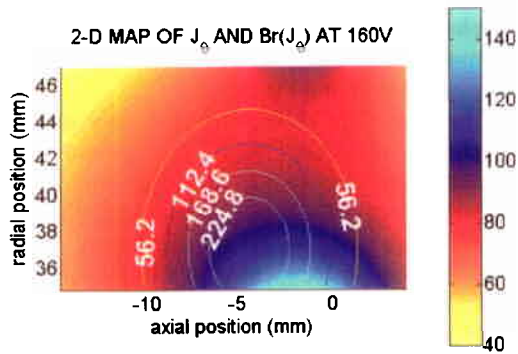


**Figure 5.** The average azimuthal drift and  $|B|$  for 160V discharge, including the contribution due to  $B(J_\theta)$ . The azimuthal drift is given by the contours in  $(\text{kA}/\text{m}^2)$ . The shaded 2-D background is  $|B|$  in (G).

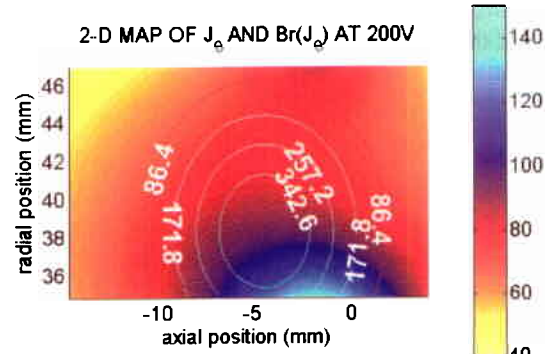


**Figure 7.** The average azimuthal drift and  $|B|$  for 200V discharge, including the contribution due to  $B(J_\theta)$ . The azimuthal drift is given by the contours in  $(\text{kA}/\text{m}^2)$ . The shaded 2-D background is  $|B|$  in (G).

currents situated at different points across the channel. It is witnessed at 200V that the maximum magnetic field is again depressed with respect to the vacuum value and shifted towards the anode. These effects are stronger than for the 160V discharge case, as one would expect since the Hall dipole is roughly 2 times greater. As a final note regarding the results thus far, it should be known that the magnetic field perturbation due to the drift current is also seen to redirect local magnetic field vectors, and appeared to do so markedly at the exit plane of the SHT. If the magnetic field lines are taken to be electrostatic equipotentials, the results of this study suggest that including the drift current in the calculation of  $B$  can shift the  $B$  field lines such that the local electric field vector near the exit plane points more sharply into the ceramic channel than would otherwise be expected. This could account for some component of increased sputtering near the exit plane, but more study will be needed to properly quantify the relative importance of the effect.

#### IV.3. Centerline Values of $J_\theta$ , $|B|$ , and $E$

To provide a more complete understanding of the axial field topology within an operating Hall thruster the centerline values of azimuthal drift, magnetic field, and electric field are provided at 160V and 200V discharge. While radially averaged values could have been provided for the non-intrusive azimuthal drift and magnetic field, values for the electric field were only collected on the centerline [5], and so, the centerline is chosen for comparative purposes. Centerline values can also be said to represent a qualitative radial average for the parameters of interest within the Hall thruster (if not a strict average). In Fig. 8 and Fig. 9 the antenna measured azimuthal drift,  $J_{ANT}$ , the intrusively estimated azimuthal drift,  $J_{INT}$ , the electric field,  $E$ , the magnitude of the vacuum magnetic field,  $B_{vac}$ , and the magnitude of the magnetic field including the contribution due to azimuthal drift,  $B(J_\theta)$ , are shown.

Discounting small registration errors in the experimental measurements of  $\sim 1$ mm, and similar numerical errors in the non-intrusive measurement of drift current, it can be concluded that the peak in electric field, magnetic field including the azimuthal drift, and azimuthal drift are co-located within the range of error in axial position. It should be noted that the vacuum value of maximum radial magnetic field is too near the exit plane, and that including the azimuthal drift shifts the maximum magnetic

field towards the anode until it more closely overlaps the maximum electric field. As a result, it can be reasonably concluded that the location of the maximum radial vacuum magnetic field is not a highly accurate predictor of the location of the maximum electric field, nor of the smallest cross-field diffusion coefficient. As a result, it is suggested that numerical models should include the azimuthal drift contribution to magnetic field if possible. The importance of this is highlighted by the fact that at 160V discharge the perturbation in the maximum radial magnetic field due to the drift was 7%, and at 200V was 12%. This does not include the added effect of fluctuations in the azimuthal drift.

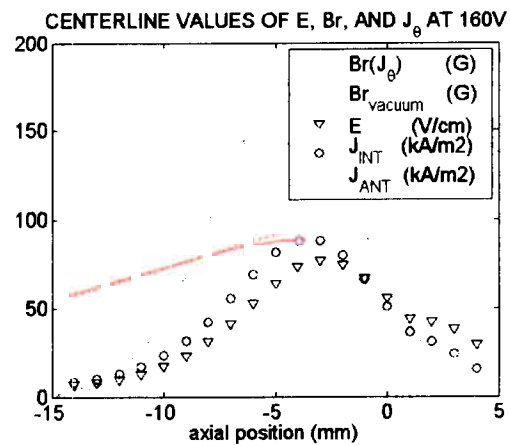


Figure 9. Centerline properties for 200V discharge.

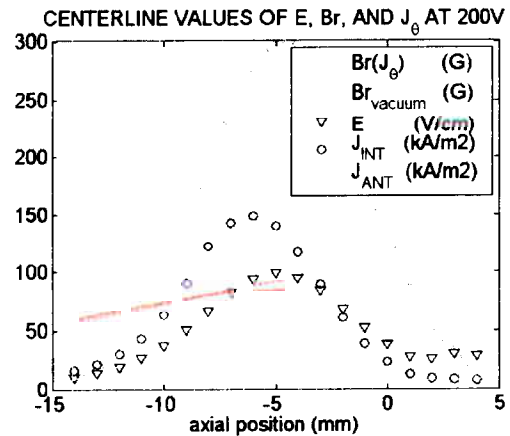


Figure 8. Centerline properties for 160V discharge.

The intrusive and non-intrusive measurements of the azimuthal drift agree closely in location and half-width, but are disparate by a factor of

two or more. By virtue of numerical simulations of the forward and reverse antenna diagnostic it is expected that the non-intrusive measurement of the azimuthal drift reported here is correct to approximately 10%. The intrusive estimate of the azimuthal drift in this study is less accurate, as it depends on measurements of the plasma potential and number density (easily incorrect by a factor of two or more) and the vacuum magnetic field, which has been shown to deviate from the operating value.

## V. SUMMARY

Fast current interruption, a novel non-invasive method for investigating the azimuthal drift in a Hall thruster, is examined as a diagnostic tool using an antenna array. The magnitude and distribution of the azimuthal drift are determined to high accuracy, and this is compared to intrusive estimates; they are found to qualitatively agree on location and half-width, but are off in magnitude by a factor of  $\sim 2$ . It is surmised that the technique used for the intrusive estimate of the azimuthal drift probably underestimates the Hall dipole.

The perturbation to the magnetic field topology affected by including the average azimuthal drift is calculated for the SHT at 160V and 200V operation. In the Hall thruster community it is generally assumed that the drift current only partially affects the magnetic field within an operating Hall thruster – and this is not born out by the results of this study. It is found that including the magnetic field perturbation caused by the azimuthal drift can shift the point of the maximum magnetic field (and does so in a way that the maximum electric field is more closely aligned with the maximum B), and depresses the magnitude of the maximum magnetic field in upwards of 15% for the operating conditions investigated.

Future research is planned to investigate the distributed Hall parameter, instabilities in the Hall drift, and their relation to one another.

## Acknowledgements

Funding for this research was provided by the Air Force Office of Scientific Research. N. Gascon was supported by a fellowship from the European Space Agency. C. Thomas received support from the National Science Foundation, and from Stanford University through the Stanford Graduate Fellowship Program.

## References

- [1]V.N. Dem'yanenko, I.P. Zubkov, S.V. Lebedev, and A.I. Morozov, "Induction method for measuring the azimuthal drift current in a Hall-current accelerator", *Sov. Phys. Tech. Phys.* 23(3), pp. 376-377, March 1978.
- [2]A.I. Bugrova, V.S. Versotskii, and V.K. Kharchevnikov, "Determination of the radial center of gravity of an azimuthal drift current in accelerators with closed electron drift", *Sov. Phys. Tech. Phys.* 25(10), pp. 1307-1308, October 1980.
- [3]Mathieu Prioul, André Bouchoule, et al., "Insights on the physics of Hall thrusters through fast current interruptions and discharge transients", 27<sup>th</sup> International Electric Propulsion Conference, IEPC-01-059.
- [4]A.I. Bugrova, A.I. Morozov, and V.K. Kharchevnikov, "Probe measurements of drift current in a Hall accelerator", *Sov. Phys. Tech. Phys.* 30(6), pp. 610-612, June 1985.
- [5]N.B. Meezan, W.A. Hargus, and M.A. Cappelli, "Optical and electrostatic characterization of oscillatory Hall discharge behavior", AIAA-98-3502, 34<sup>th</sup> Joint Propulsion Conference, Cleveland, OH, July 1998.
- [6]W.A. Hargus and M.A. Cappelli, "Laser induced fluorescence measurements on a laboratory Hall thruster", AIAA Paper No. 98-3645, 34<sup>th</sup> Joint Propulsion Conference, Cleveland, OH, July 1998.
- [7]W.A. Hargus, "Investigation of the plasma acceleration mechanism within a co-axial Hall thruster", Ph.D. Thesis, Mechanical Engineering Department, Stanford University, 2001.
- [8]P.Y. Peterson, A.D. Gallimore, J.M. Haas, "An experimental investigation of the internal magnetic field topography of an operating Hall thruster", *Physics of Plasmas*, Volume 9, No. 10, Oct 2002, pp.
- [9]C.A. Thomas, N. Gascon, M.A. Cappelli, "A Study of the azimuthal drift in an ExB discharge using a non-invasive antenna array", AIAA Paper No. ????, 39<sup>th</sup> Joint Propulsion Conference, Huntsville, AL, July 2003.
- [10] <http://femm.foster-miller.net/>